A full-probabilistic cloud analysis for structural seismic fragility via decoupled M-PDEM

Meng-Ze Lyu [a,b], De-Cheng Feng [c,d,*], Xu-Yang Cao [e], Michael Beer [f,g,h,i]

[a] State Key Lab. of Disaster Reduction in Civil Engineering, Tongji University, 1239 Siping Rd., Shanghai 200092, China
[b] College of Civil Engineering, Tongji University, 1239 Siping Rd., Shanghai 200092, China
[c] Key Lab. of Concrete & Prestressed Concrete Structures of the Ministry of Education, Southeast University, 2 Sipailou, Nanjing 210096, China
[d] School of Civil Engineering, Southeast University, 2 Sipailou, Nanjing 210096, China
[e] College of Civil & Transportation Engineering, Hohai University, 1 Xikang Rd., Nanjing 210098, China
[f] Institute for Risk & Reliability, Leibniz Universität Hannover, 34 Carlinstr., Hannover 30167, Germany
[g] Institute for Risk & Uncertainty, University of Liverpool, Peach Str. Chadwick Building, Liverpool L69 7ZF, UK
[h] International Joint Research Center for Engineering Reliability & Stochastic Mechanics, Tongji University, 1239 Siping Rd., Shanghai 200092, China
[i] International Joint Research Center for Resilient Infrastructure, Tongji University, 1239 Siping Rd., Shanghai 200092, China
[*] Corresponding author
E-mail: lyumz@tongji.edu.cn (M. Z. Lyu), dcfeng@seu.edu.cn (D. C. Feng), caoxy@hhu.edu.cn (X. Y. Cao), beer@irz.uni-hannover.de (M. Beer)

Abstract

Performance-based earthquake engineering (PBEE) is essential for ensuring engineering safety. Conducting seismic fragility analysis within this framework is imperative. Existing methods for seismic fragility analysis often rely heavily on double loop reanalysis and empirical data fitting, leading to challenges in obtaining high-precision results with a limited number of representative structural analysis instances. In this context, a new methodology for seismic fragility based on a full-probabilistic cloud analysis is proposed via the decoupled multi-probability density evolution method (M-PDEM). In the proposed method, the assumption of a log-normal distribution is not required. According to the random event description of the principle of preservation of probability, the transient probability density functions (PDFs) of intensity measure (IM) and engineering demand parameter (EDP), as key response quantities of the seismic-structural system, are governed by one-dimensional Li-Chen equations, where the physics-driven forces are determined by representative analysis data of the stochastic dynamic system. By generating ground motions based on representative points of basic random variables and performing structural dynamic analysis, the decoupled M-PDEM is employed to solve the one-dimensional Li-Chen equations. This yields the joint PDF of IM and EDP, as well as the conditional PDF of EDP given IM, resulting in seismic fragility analysis outcomes. The numerical implementation procedure is elaborated in detail, and validation is performed using a six-story nonlinear reinforced concrete (RC) frame subjected to non-stationary stochastic ground motions. Comparative analysis against Monte Carlo simulation (MCS) and traditional cloud analysis based on least squares regression (LSR) reveals that the proposed method achieves higher computational precision at comparable structural analysis costs. By directly solving the physics-driven Li-Chen equations, the method provides the full-probabilistic joint information of IM and EDP required for cloud analysis, surpassing the accuracy achieved by traditional methods based on statistical moment fitting and empirical distribution assumptions.

Keywords: Seismic fragility; Full-probabilistic cloud analysis; Performance-based earthquake engineering (PBEE); Li-Chen equation; Decoupled multi-probability density evolution method (M-PDEM).

1. Introduction

Performance-based earthquake engineering (PBEE) stands as a cornerstone in ensuring the resilience of structures against seismic events, encompassing strategies to predict, mitigate, and reduce seismic risks, enhance structural safety, and minimize post-earthquake property losses (Priestley 2000, Porter 2003, Moehle & Deierlein 2004). Within this context, seismic fragility analysis plays a pivotal role, enabling the assessment of structural vulnerability and informing decision-making processes aimed at safeguarding human lives and critical infrastructure (Shinozuka et al. 2000, Gardoni et al. 2002, Choi et al. 2004, Ellingwood et al. 2004).

Seismic fragility assessment methodologies are classified into three main categories: multiple support analysis (MSA), incremental dynamic analysis (IDA), and cloud analysis. MSA (Singhal & Kiremidjian 1996) and IDA (Vamvatsikos & Cornell 2002) involve iterative structural re-analyses across various intensity measure (IM) levels, inherently confronting the computational burden of the double-loop problem (Jia & Taflanidis 2014, Gasser et al. 2019), namely, it is necessary to conduct numerous representative analyses at each IM level, while simultaneously iterating through all IMs (Baker 2015, Pang & Wang 2021, Wang et al. 2022, Luo & Ai 2023, Lyu et al. 2023a). Conversely, cloud analysis (Cornell et al. 2002) offer computational efficiency but often rely on empirical distribution fitting of statistical moments, e.g., least squares regression (LSR) for log conditional means and standard deviation (STD), to approximate the conditional probability density functions (PDFs) of engineering demand parameter (EDP) given IM (Nielson & DesRoches 2007, Padgett et al. 2008, Jalayer et al. 2015, Cao et al. 2023c). To make the concept of fragility more comprehensive, there have been new developments fragility assessment models involving vector-valued IMs (Shafieezadeh et al. 2012, Zhou et al. 2017, Du & Padgett 2020) and in multiple damage states (Jalayer et al. 2023). However, the above cloud-based approaches may lead to inadequate accuracy in capturing the complex relationships and evolving characteristics of IM and EDP joint distributions, particularly in regions of low probability where the fit of the log-normal distribution is less accurate. This limitation arises due to the reliance on statistical moments without fully considering the underlying physical mechanisms driving the joint evolution of IMs and EDPs under varying seismic conditions. As such, there exists a compelling need to develop a comprehensive probabilistic cloud analysis method that ensures both accuracy and computational tractability.

The current landscape of cloud analysis-based fragility assessment develops various non-parametric approaches, directly estimating the joint probability distributions of IMs and EDPs driven by analysis data (Lallemant et al. 2015, Feng et al. 2023, Cao et al. 2023a). These methods encompass a range of techniques, including direct Monte Carlo simulation (MCS) combined with kernel density estimation (Mai et al. 2017, Cao et al. 2023b), clustering algorithms paired with polynomial kernels (Altieri & Patelli 2020), as well as the incorporation of diverse surrogate models or machine learning techniques (Mangalathu et al. 2018, Wang et al. 2018, Kiani et al. 2019). However, the integration of physical mechanisms governing the evolution of joint probability distributions under stochastic seismic excitation remains largely unexplored. As seismic forces interact with structural systems, IM and EDP become dependent stochastic processes influenced by basic random variables of the seismic-structural system, such as stochastic structural and seismic parameters. The evolution of their PDFs over time should be governed by a set of partial differential equations (PDEs), known as the Li-Chen equations (Nielsen et al. 2016).

The seminal work of Li and Chen (2008) established the principle of preservation of probability for physical stochastic systems, culminating in the derivation of the Li-Chen equations that govern the transient PDFs of arbitrary quantities of interest in complex nonlinear dynamic systems (Li & Chen 2008, Chen & Li 2009). Importantly, the dimensionality of the Li-Chen equations is solely dependent on the dimensionality of the interested quantity, unaffected by the system's degrees of freedom (DOFs) or the number of random variables involved. This exceptional feature enables efficient high-dimensional stochastic response analysis, giving rise to the methodology of probability density evolution method (PDEM) (Li & Chen 2009, Li et al. 2012, Lyu & Chen 2022). The accuracy and

effectiveness of PDEM have been rigorously examined through theoretical investigations and numerical validations (Chen et al. 2016, 2020b, Li & Wang 2022), demonstrating its capability to capture intricate probabilistic behaviors of complex systems. Furthermore, PDEM has found wide applications in various engineering domains, facilitating studies on uncertainty propagation (Papadopoulos & Kalogeris 2016, Hai & Lyu 2023, Liu & Lyu 2023) and reliability analysis (Afshari & Pourtakdoust 2018, Ang et al. 2021, Lyu et al. 2023b). Recent advancements (Lyu et al. 2024) suggest that joint PDFs of multiple response quantities can be realized through the solution of decoupled one-dimensional Li-Chen equations, further reducing the computational complexity of time-variant joint PDF analysis.

Key to cloud analysis-based fragility assessment is the acquisition of the joint distribution of IMs and EDPs, a challenge adeptly addressed by the decoupled multi-PDEM (M-PDEM). Within this framework, the Li-Chen equations provide a physically-driven evolution of the joint PDF of IM and EDP under stochastic seismic actions, data-informed by representative structural dynamic analyses. This methodology facilitates efficient and refined full-probabilistic seismic fragility analysis.

The logical framework of this paper unfolds as follows: Sec. 2 outlines the foundational principles of cloud-based fragility assessment; Sec. 3 details the methodology of determining joint and conditional PDFs of IM and EDP through the decoupled M-PDEM; Sec. 4 presents the numerical implementation procedure; Sec. 5 showcases the validation of the proposed method using a benchmark nonlinear reinforced concrete (RC) frame subjected to non-stationary stochastic ground motions; Sec. 6 discusses the results and highlights the method's advantages; and finally, Sec. 7 provides concluding remarks.

2. Probabilistic perspective of cloud-based fragility analysis

2.1. Description of classical cloud analysis

Cloud analysis (Cornell et al. 2002) is a classical approach to assess the seismic fragility of engineering structures via determining the probability of EDP exceeding threshold limits under various values of seismic IM. Earthquake ground motion exhibits strong stochasticity, and the IM can be regarded as a random variable. If the stochastic ground motion with a realization of IM is applied as input to a structure, the EDP of the structure remain random due to the overall randomness of ground motion. Cloud analysis posits a linear conditional expectation relationship between the two random variables, IM and EDP (Cornell et al. 2002), namely,

$$\hat{\mu}_{\ln \mathrm{D}}\left(x\right)=\mathrm{E}\left(\ln EDP\middle|\, IM=x\right)=\hat{\alpha}+\hat{\beta}\ln x, \tag{1}$$

where x is a realization of IM; $\hat{\alpha}$ and $\hat{\beta}$ are coefficients estimated by the LSR according to a series of sample pairs of IM and EDP, i.e.,

$$\left(\hat{\alpha},\hat{\beta}\right)=\underset{(\alpha,\beta)}{\arg\min}\left\{\sum_{i=1}^{n}\left(\alpha+\beta\ln\tilde{x}_i-\ln\tilde{z}_i\right)^2\right\}, \tag{2}$$

in which $\left(\tilde{x}_i,\tilde{z}_i\right)$, for $i=1,...,n$, is n sample pairs of IM and EDP given by deterministic structural analyses.

Furthermore, assume that the EDP follows a lognormal distribution for each realization of IM as a condition (Padgett et al. 2008, Jalayer & Cornell 2009), namely,

$$EDP_{|IM=x}\sim\mathcal{LN}\left(\hat{\mu}_{\ln \mathrm{D}}\left(x\right),{\hat{\sigma}_{\ln \mathrm{D}}}^2\right), \tag{3}$$

where $\hat{\mu}_{\ln \mathrm{D}}\left(x\right)$ is the logarithmic mean given by Eq. (1); $\hat{\sigma}_{\ln \mathrm{D}}$ is the logarithmic STD considered to be constant and estimated from the sample pairs of IM and EDP as

$$\hat{\sigma}_{\ln \mathrm{D}}=\sqrt{\frac{1}{n-2}\sum_{i=1}^{n}\left[\ln \tilde{z}_i-\hat{\mu}_{\ln \mathrm{D}}\left(\tilde{x}_i\right)\right]^2}. \tag{4}$$

Then, the fragility function at a given threshold b of EDP can be estimated as

$$F\left(x;b\right)=\Pr\left\{EDP\geqslant b\middle|\ IM=x\right\}=\Phi\left(\frac{\hat{\alpha}+\hat{\beta}\ln x-\ln b}{\hat{\sigma}_{\ln \mathrm{D}}}\right), \tag{5}$$

where $\Phi\left(\cdot\right)$ is the standard Gaussian cumulative distribution function (CDF).

In the classic procedure of the above cloud analysis, three assumptions are employed:

(1) The linear correlation assumption, which considers that the logarithms of IM and EDP have a linear conditional expectation relationship;

(2) The conditional distribution assumption, which assumes that the conditional probability distribution of EDP given any realization of IM follows a log-normal distribution;

(3) The conditional variance assumption, which assumes that the conditional variance of the logarithms of EDP given any realization x of IM remains constant and does not vary with x.

These three assumptions heavily rely on empirical observations and do not account for the differences in the physical stochastic characteristics of seismic motion in various engineering sites or the distinct physical-mechanical properties of different engineering structures. Consequently, fragility curves obtained solely through statistical fitting based on empirical assumptions are inherently limited in accuracy. Therefore, addressing how to perform physically realistic probabilistic seismic vulnerability analysis based on the concept of the cloud analysis method remains a challenge.

2.2. Full-probabilistic perspective of cloud analysis

The essence of the cloud analysis method lies in calculating the fragility function through the conditional probability of EDP given various realizations of the IM. If the conditional PDF of EDP given IM is available, denoted as $p_{\mathrm{EDP|IM}}\left(z\middle|x\right)$, the conditional probability can be obtained by numerically integrating the conditional PDF, namely,

$$F\left(x;b\right)=\Pr\left\{EDP\geqslant b\middle|\ IM=x\right\}=\int_b^{\infty}p_{\mathrm{EDP|IM}}\left(z\middle|x\right)\mathrm{d}z, \tag{6}$$

where the conditional PDF can be given as

$$p_{\mathrm{EDP|IM}}\left(z\middle|x\right)=\frac{p_{\mathrm{IM,EDP}}\left(x,z\right)}{p_{\mathrm{IM}}\left(x\right)}, \tag{7}$$

in which $p_{\mathrm{IM}}\left(x\right)$ is the PDF of IM; $p_{\mathrm{IM,EDP}}\left(x,z\right)$ is the joint PDF of IM and EDP.

Therefore, achieving cloud-based seismic fragility analysis under the full-probabilistic perspective requires obtaining the joint PDF of the two key response quantities, IM and EDP, in the complex nonlinear stochastic dynamic system of "earthquake-structure". In this framework, the classical cloud analysis based on the above three assumptions provides only a specific parametric form of the conditional PDF, namely a lognormal distribution as

$$p_{\mathrm{EDP|IM}}\left(z\middle|x\right)=\frac{1}{\sqrt{2\pi}\hat{\sigma}_{\ln \mathrm{D}}z}e^{-\frac{\left(\ln z-\hat{\alpha}-\hat{\beta}\ln x\right)^2}{2\hat{\sigma}_{\ln \mathrm{D}}{}^2}},\ \text{for } z\geqslant 0. \tag{8}$$

Additionally, previous studies by Mai et al. (2017) and Cao et al. (2023b) have explored non-parametric approaches based on kernel density estimation using sample data. However, direct fitting at the data level is limited in capturing

the physics-driven evolution of probabilistic dependencies during the uncertainty propagation from earthquake (e.g., IM) to structure (e.g., EDP). This evolution is the intrinsic reason behind the strong probabilistic correlation between IM and EDP. Introducing the PDEM may offer deeper insights to address this issue.

3. Conditional PDF determination via decoupled M-PDEM

3.1. Probability density evolution method

Without loss of generality, a complex nonlinear structure subjected to non-stationary stochastic ground motion can be modeled as the high-dimensional stochastic dynamical system with the equation of motion as

$$\mathbf{M}\left(\boldsymbol{\Theta}\right)\ddot{\mathbf{Y}}\left(t\right)+\mathbf{f}\left[\mathbf{Y}\left(t\right),\dot{\mathbf{Y}}\left(t\right),\boldsymbol{\Theta},t\right]=-\mathbf{M}\left(\boldsymbol{\Theta}\right)\mathbf{1}_{m}\xi\left(\boldsymbol{\Theta},t\right), \tag{9}$$

where $\mathbf{Y}\left(t\right)$, $\dot{\mathbf{Y}}\left(t\right)$, and $\ddot{\mathbf{Y}}\left(t\right)$ are the m-dimensional displacement, velocity, and acceleration response process vector, and m is the number of the DOFs; $\boldsymbol{\Theta}$ is the basic random vector involving the randomness both from structural parameters and ground motions with the known joint PDF $p_{\boldsymbol{\Theta}}\left(\boldsymbol{\theta}\right)$; $\xi\left(\boldsymbol{\Theta},t\right)$ is the non-stationary stochastic ground motion excitation process with the duration $t\in\left[0,t_{\mathrm{f}}\right]$; $\mathbf{M}\left(\boldsymbol{\Theta}\right)$ is the $m\times m$ mass matrix; $\mathbf{f}\left(\cdot\right)$ is the m-dimensional nonlinear damping and restoring force vector function.

When the basic random vector $\boldsymbol{\Theta}$ takes any realization $\boldsymbol{\theta}$, Eq. (9) becomes a deterministic nonlinear dynamic system that can be numerically solved to obtain the deterministic time history of any desired response quantity $Z\left(t\right)$ in the system. Therefore, with $\boldsymbol{\Theta}$ serving as uncertain inputs, $Z\left(t\right)$ can be considered as a deterministic function of both the basic random vector $\boldsymbol{\Theta}$ and time t, namely,

$$Z\left(t\right)=g\left(\boldsymbol{\Theta},t\right), \tag{10}$$

where $g\left(\cdot\right)$ is a deterministic function that does not have an explicit expression and can be determined with various realization $\boldsymbol{\theta}$ by solving Eq. (9) numerically; $Z\left(t\right)$ represents any quantity of interest, which can be a specific function or functional of seismic and structural responses within the system, i.e., $Z\left(t\right)=\mathcal{L}\left[\mathbf{Y}\left(t\right),\xi\left(\boldsymbol{\Theta},t\right)\right]$ in which $\mathcal{L}\left(\cdot\right)$ is a function or functional operator.

Eq. (10) actually constitutes the physical basis for random events description in the principle of preservation of probability. Under this description, based on the principle of preservation of probability, it can be derived that the joint PDF of $Z\left(t\right)$ and $\boldsymbol{\Theta}$, denoted as $p_{Z\boldsymbol{\Theta}}\left(z,\boldsymbol{\theta},t\right)$, satisfies the Li-Chen equation (Li & Chen 2008, Chen & Li 2009), namely,

$$\frac{\partial p_{Z\boldsymbol{\Theta}}\left(z,\boldsymbol{\theta},t\right)}{\partial t}+\dot{g}\left(\boldsymbol{\theta},t\right)\frac{\partial p_{Z\boldsymbol{\Theta}}\left(z,\boldsymbol{\theta},t\right)}{\partial z}=0, \tag{11}$$

where $\dot{g}\left(\boldsymbol{\theta},t\right)$ is the derivative of $g\left(\boldsymbol{\Theta},t\right)$ with respect to t under a given $\boldsymbol{\Theta}=\boldsymbol{\theta}$. The detailed proof of Eq. (11) can be found in Li and Chen (2008).

Solving Li-Chen equation (11) with each realization $\boldsymbol{\theta}$ yields the numerical solution of $p_{Z\boldsymbol{\Theta}}\left(z,\boldsymbol{\theta},t\right)$. Then, integrating $p_{Z\boldsymbol{\Theta}}\left(z,\boldsymbol{\theta},t\right)$ with respect to $\boldsymbol{\theta}$ yields the transient PDF of $Z\left(t\right)$, namely,

$$p_{Z}\left(z,t\right)=\int_{\mathbb{R}^{s}}p_{Z\boldsymbol{\Theta}}\left(z,\boldsymbol{\theta},t\right)\mathrm{d}\boldsymbol{\theta}, \tag{12}$$

where $\mathbb{R}^{s}$ is the s-dimensional real domain, and s is the dimension of $\boldsymbol{\Theta}$. This constitutes the fundamental framework of the PDEM (Li & Chen 2004, Li et al. 2012, Chen et al. 2016).

3.2. Decoupled M-PDEM for cloud analysis

For the general case of seismic fragility analysis of complex nonlinear structures, the peak ground acceleration (PGA) of stochastic seismic motion can be employed as the IM, while the maximum inter-story drift angle (MIDA) of all floors of the structure can serve as the EDP. In this scenario, the logarithms of the time-variant extreme values processes of PGA and MIDA can be regarded as the quantities of interest, namely,

$$\begin{cases} Z_{\mathrm{IM}}\left(t\right)=\ln\left[\max\limits_{0\leqslant\tau\leqslant t}\left\{\left|\xi\left(\boldsymbol{\Theta},\tau\right)\right|\right\}\right], \\ Z_{\mathrm{EDP}}\left(t\right)=\ln\left[\max\limits_{0\leqslant\tau\leqslant t}\left\{\max\limits_{i=1,\ldots,m}\left\{\dfrac{\left|Y_i\left(\tau\right)-Y_{i-1}\left(\tau\right)\right|}{h_i}\right\}\right\}\right], \end{cases} \tag{13}$$

where h_i is the height of the i-th story; $Y_0\left(\tau\right)=0$ is forcibly defined. The logarithms of IM and EDP required for the fragility analysis are the values of these quantities of interest at the termination time t_{f}, i.e.,

$$\ln IM=Z_{\mathrm{IM}}\left(t_{\mathrm{f}}\right)\text{and}\ln EDP=Z_{\mathrm{EDP}}\left(t_{\mathrm{f}}\right), \tag{14}$$

respectively.

Remark 1: Of course, apart from the PGA, other measures such as the spectral acceleration can also be chosen as the IM. Since the proposed method is non-parametric, there is no need to consider linear regression errors for the IM selection. The selection of PGA as the IM is primarily due to its structure-independence and its ability to better reflect the inherent characteristics of the earthquake. In addition, besides the MIDA, other alternative performance indicators can also be chosen according to engineering requirements. In Eqs. (13) and (14), the logarithmic operation can also be omitted simultaneously. However, numerical experiments have shown that using the logarithmically transformed values as the quantities of interest yields more accurate numerical analysis results.

According to Eq. (11), the joint PDF of $Z_{\mathrm{IM}}\left(t\right)$ or $Z_{\mathrm{EDP}}\left(t\right)$ and $\boldsymbol{\Theta}$ satisfies the Li-Chen equation, namely,

$$\begin{cases} \dfrac{\partial p_{Z_{\mathrm{IM}}\boldsymbol{\Theta}}\left(z_1,\boldsymbol{\theta},t\right)}{\partial t}+\dot{g}_{\mathrm{IM}}\left(\boldsymbol{\theta},t\right)\dfrac{\partial p_{Z_{\mathrm{IM}}\boldsymbol{\Theta}}\left(z_1,\boldsymbol{\theta},t\right)}{\partial z_1}=0, \\ \dfrac{\partial p_{Z_{\mathrm{EDP}}\boldsymbol{\Theta}}\left(z_2,\boldsymbol{\theta},t\right)}{\partial t}+\dot{g}_{\mathrm{EDP}}\left(\boldsymbol{\theta},t\right)\dfrac{\partial p_{Z_{\mathrm{EDP}}\boldsymbol{\Theta}}\left(z_2,\boldsymbol{\theta},t\right)}{\partial z_2}=0, \end{cases} \tag{15}$$

where $g_{\mathrm{IM}}\left(\boldsymbol{\theta},t\right)$ and $g_{\mathrm{EDP}}\left(\boldsymbol{\theta},t\right)$ are the deterministic solutions of $Z_{\mathrm{IM}}\left(t\right)$ and $Z_{\mathrm{EDP}}\left(t\right)$ obtained by solving Eq. (9) at the realization $\boldsymbol{\Theta}=\boldsymbol{\theta}$, respectively. The marginal PDFs of $Z_{\mathrm{IM}}\left(t\right)$ and $Z_{\mathrm{EDP}}\left(t\right)$ can be obtained by integrating the solutions of Li-Chen equations (15) with respect to $\boldsymbol{\theta}$. However, how does one derive the joint PDF of $Z_{\mathrm{IM}}\left(t\right)$ and $Z_{\mathrm{EDP}}\left(t\right)$ required for the fragility analysis as in Eq. (7)?

According to the decoupled M-PDEM (Lyu et al. 2024), for any realization $\boldsymbol{\theta}$, there is

$$p_{Z_{\mathrm{IM}}Z_{\mathrm{EDP}}\boldsymbol{\Theta}}\left(z_1,z_2,\boldsymbol{\theta},t\right)=\frac{p_{Z_{\mathrm{IM}}\boldsymbol{\Theta}}\left(z_1,\boldsymbol{\theta},t\right)p_{Z_{\mathrm{EDP}}\boldsymbol{\Theta}}\left(z_2,\boldsymbol{\theta},t\right)}{p_{\boldsymbol{\Theta}}\left(\boldsymbol{\theta}\right)}. \tag{16}$$

Note that due to the correlation between IM and EDP, the joint PDF cannot be expressed directly as the product of individual marginal PDFs. However, based on the random event description of the principle of preservation of probability (Lyu et al. 2024), under each $\boldsymbol{\Theta}=\boldsymbol{\theta}$, the joint PDF of multiple responses can be calculated by multiplying the PDFs of each response. The detailed proof of Eq. (16) can be found in Lyu et al. (2024). Then, the joint PDF of $Z_{\mathrm{IM}}\left(t\right)$ and $Z_{\mathrm{EDP}}\left(t\right)$ can be given as

$$p_{Z_{\mathrm{IM}}Z_{\mathrm{EDP}}}\left(z_1,z_2,t\right)=\int_{\mathbb{R}^s}p_{Z_{\mathrm{IM}}Z_{\mathrm{EDP}}\boldsymbol{\Theta}}\left(z_1,z_2,\boldsymbol{\theta},t\right)\mathrm{d}\boldsymbol{\theta}. \tag{17}$$

According to Eq. (14), the joint PDF of IM and EDP can be given as

$$p_{\mathrm{IM,EDP}}\left(x,z\right)=\frac{p_{Z_{\mathrm{IM}}Z_{\mathrm{EDP}}}\left(\ln x,\ln z,t_{\mathrm{f}}\right)}{xz},\text{for } x,z>0, \tag{18}$$

and the conditional PDF of EDP with given IM is

$$p_{\mathrm{EDP|IM}}\left(z\middle|x\right)=\frac{p_{Z_{\mathrm{EDP}}|Z_{\mathrm{IM}}}\left(\ln z\middle|\ln x,t_{\mathrm{f}}\right)}{z}=\frac{p_{Z_{\mathrm{IM}}Z_{\mathrm{EDP}}}\left(\ln x,\ln z,t_{\mathrm{f}}\right)}{zp_{Z_{\mathrm{IM}}}\left(\ln x,t_{\mathrm{f}}\right)},\text{for } x,z>0. \tag{19}$$

Then, according to Eqs. (16) to (19), the fragility function in Eq. (6) can be captured via the solution of Li-Chen equations (15) as

$$\begin{aligned}F\left(x;b\right)&=\int_b^\infty p_{\mathrm{EDP|IM}}\left(z\middle|x\right)\mathrm{d}z=\int_b^\infty\frac{p_{Z_{\mathrm{IM}}Z_{\mathrm{EDP}}}\left(\ln x,\ln z,t_{\mathrm{f}}\right)}{zp_{Z_{\mathrm{IM}}}\left(\ln x,t_{\mathrm{f}}\right)}\mathrm{d}z\\&=\frac{1}{\int_{\mathbb{R}^s}p_{Z_{\mathrm{IM}}\boldsymbol{\Theta}}\left(\ln x,\boldsymbol{\theta},t_{\mathrm{f}}\right)\mathrm{d}\boldsymbol{\theta}}\int_b^\infty\frac{1}{z}\int_{\mathbb{R}^s}p_{Z_{\mathrm{IM}}Z_{\mathrm{EDP}}\boldsymbol{\Theta}}\left(\ln x,\ln z,\boldsymbol{\theta},t_{\mathrm{f}}\right)\mathrm{d}\boldsymbol{\theta}\mathrm{d}z\\&=\frac{1}{\int_{\mathbb{R}^s}p_{Z_{\mathrm{IM}}\boldsymbol{\Theta}}\left(\ln x,\boldsymbol{\theta},t_{\mathrm{f}}\right)\mathrm{d}\boldsymbol{\theta}}\int_b^\infty\frac{1}{z}\int_{\mathbb{R}^s}\frac{p_{Z_{\mathrm{IM}}\boldsymbol{\Theta}}\left(\ln x,\boldsymbol{\theta},t_{\mathrm{f}}\right)p_{Z_{\mathrm{EDP}}\boldsymbol{\Theta}}\left(\ln z,\boldsymbol{\theta},t_{\mathrm{f}}\right)}{p_{\boldsymbol{\Theta}}\left(\boldsymbol{\theta}\right)}\mathrm{d}\boldsymbol{\theta}\mathrm{d}z.\end{aligned} \tag{20}$$

Eq. (20) provides the main formula for conducting the cloud-based fragility analysis through the decoupled M-PDEM. The term "decoupled" refers to the approach of obtaining the joint PDF of IM and EDP in cloud analysis without directly solving the high-dimensional probability density evolution equation for the coupling of IM and EDP. Instead, it involves solving the one-dimensional probability density evolution equations for IM and EDP separately for each representative realization of $\boldsymbol{\theta}$.

4. Numerical implementation procedure

The specific numerical implementation procedure of the cloud-based fragility analysis via the decoupled M-PDEM includes the following four steps:

Step 1. Partitioning the probabilistic space of basic random vector.

First, determine the basic random vector $\boldsymbol{\Theta}$ that reflects the randomness of the structural parameters and seismic excitations, such as the mass and initial stiffness of each story, and random frequencies and phases of each harmonic term required for seismic generation, etc. Appropriate numerical techniques are utilized to discretize the probability space of $\boldsymbol{\Theta}$, obtaining a series of representative points $\boldsymbol{\theta}^{(q)}$, for $q=1,...,n$. A representative point selection strategy based on the generalized F-discrepancy can be employed here (Chen et al. 2016).

Subsequently, the assigned probabilities for each representative point $\boldsymbol{\theta}^{(q)}$ can be determined as

$$P_q=\int_{\Omega^{(q)}}p_{\boldsymbol{\Theta}}\left(\boldsymbol{\theta}\right)\mathrm{d}\boldsymbol{\theta}, \tag{21}$$

where $\Omega^{(q)}$ is the probabilistic subdomain of $\boldsymbol{\theta}^{(q)}$ in the probabilistic space, and can be defined by the Voronoi cell (Chen et al. 2009).

Then, a series of representative non-stationary seismic ground acceleration histories corresponding to the representative points can be generated and denoted as $\xi\left(\boldsymbol{\theta}^{(q)},t\right)$ in $t\in\left[0,t_{\mathrm{f}}\right]$, for $q=1,...,n$. To reduce the dimensionality of $\boldsymbol{\Theta}$, the stochastic harmonic function (SHF) can be used to generate seismic excitations (Chen et

al. 2013, 2017). For detailed seismic excitation modeling and characterization, refer to Subsec. 5.1. The representative history of quantity of interest corresponding to IM can be determined as $Z_{\mathrm{IM}}(t)=g_{\mathrm{IM}}\left(\boldsymbol{\theta}^{(q)},t\right)$, for $q=1,...,n$, e.g., according to the first equation in Eq. (13).

Step 2. Performing representative seismic dynamic analyses of the structure.

The representative seismic dynamic analyses can be performed by solving Eq. (9) numerically with each $\boldsymbol{\Theta}=\boldsymbol{\theta}^{(q)}$, for $q=1,...,n$. Various approaches for deterministic dynamic analysis can be used according to the specific problem in this step.

Then, the representative history of quantity of interest corresponding to EDP can be determined as $Z_{\mathrm{EDP}}(t)=g_{\mathrm{EDP}}\left(\boldsymbol{\theta}^{(q)},t\right)$, for $q=1,...,n$, e.g., according to the second equation in Eq. (13).

Step 3. Solving the Li-Chen equation.

Substituting $Z_{\mathrm{IM}}(t)=g_{\mathrm{IM}}\left(\boldsymbol{\theta}^{(q)},t\right)$ and $Z_{\mathrm{EDP}}(t)=g_{\mathrm{EDP}}\left(\boldsymbol{\theta}^{(q)},t\right)$ in, Li-Chen equations (15) can be solved at each $\boldsymbol{\theta}^{(q)}$ with appropriate initial conditions individually, namely solving

$$\begin{cases}\dfrac{\partial p_{Z_{\mathrm{IM}}}^{(q)}(z_1,t)}{\partial t}+\dot{g}_{\mathrm{IM}}\left(\boldsymbol{\theta}^{(q)},t\right)\dfrac{\partial p_{Z_{\mathrm{IM}}}^{(q)}(z_1,t)}{\partial z_1}=0,\\ \dfrac{\partial p_{Z_{\mathrm{EDP}}}^{(q)}(z_2,t)}{\partial t}+\dot{g}_{\mathrm{EDP}}\left(\boldsymbol{\theta}^{(q)},t\right)\dfrac{\partial p_{Z_{\mathrm{EDP}}}^{(q)}(z_2,t)}{\partial z_2}=0,\end{cases}\quad \text{for } q=1,...,n, \tag{22}$$

where $p_{Z_{\mathrm{IM}}}^{(q)}(z_1,t)$ and $p_{Z_{\mathrm{EDP}}}^{(q)}(z_2,t)$ are, respectively, the sub-PDFs of $Z_{\mathrm{IM}}(t)$ and $Z_{\mathrm{EDP}}(t)$ in the probabilistic subdomain $\Omega^{(q)}$, i.e.,

$$\begin{cases}p_{Z_{\mathrm{IM}}}^{(q)}(z_1,t)=\int_{\Omega^{(q)}}p_{Z_{\mathrm{IM}}\boldsymbol{\Theta}}(z_1,\boldsymbol{\theta},t)\,\mathrm{d}\boldsymbol{\theta}\doteq p_{Z_{\mathrm{IM}}|\boldsymbol{\Theta}}\left(z_1,t\middle|\boldsymbol{\theta}^{(q)}\right)\int_{\Omega^{(q)}}p_{\boldsymbol{\Theta}}(\boldsymbol{\theta})\,\mathrm{d}\boldsymbol{\theta}=p_{Z_{\mathrm{IM}}|\boldsymbol{\Theta}}\left(z_1,t\middle|\boldsymbol{\theta}^{(q)}\right)P_q,\\ p_{Z_{\mathrm{EDP}}}^{(q)}(z_2,t)=\int_{\Omega^{(q)}}p_{Z_{\mathrm{EDP}}\boldsymbol{\Theta}}(z_2,\boldsymbol{\theta},t)\,\mathrm{d}\boldsymbol{\theta}\doteq p_{Z_{\mathrm{EDP}}|\boldsymbol{\Theta}}\left(z_2,t\middle|\boldsymbol{\theta}^{(q)}\right)\int_{\Omega^{(q)}}p_{\boldsymbol{\Theta}}(\boldsymbol{\theta})\,\mathrm{d}\boldsymbol{\theta}=p_{Z_{\mathrm{EDP}}|\boldsymbol{\Theta}}\left(z_2,t\middle|\boldsymbol{\theta}^{(q)}\right)P_q.\end{cases} \tag{23}$$

Various numerical schemes for solving hyperbolic PDEs, i.e., Eq. (15), can be employed in this step, such as the finite difference method (Li & Chen 2004, 2009), the direct probability integral method (Fan et al. 2009, Chen & Yang 2019), the finite element method (Papadopoulos & Kalogeris 2016), the reproducing kernel particle method (Wang & Li 2020, Wang et al. 2021), or deep learning methods (Pourtakdoust & Khodabakhsh 2022, Das & Tesfamariam 2024), to obtain the sub-PDFs $p_{Z_{\mathrm{IM}}}^{(q)}(z_1,t)$ and $p_{Z_{\mathrm{EDP}}}^{(q)}(z_2,t)$.

Step 4. Calculating the joint PDF of IM-EDP and the fragility function.

According to the decoupled M-PDEM (Lyu et al. 2024), the joint PDF of IM and EDP in Eq. (18) can be calculated as

$$\begin{aligned}p_{\mathrm{IM,EDP}}(x,z)&=\frac{1}{xz}\int_{\mathbb{R}^s}\frac{p_{Z_{\mathrm{IM}}\boldsymbol{\Theta}}(\ln x,\boldsymbol{\theta},t_{\mathrm{f}})\,p_{Z_{\mathrm{EDP}}\boldsymbol{\Theta}}(\ln z,\boldsymbol{\theta},t_{\mathrm{f}})}{p_{\boldsymbol{\Theta}}(\boldsymbol{\theta})}\mathrm{d}\boldsymbol{\theta}\\ &=\frac{1}{xz}\int_{\mathbb{R}^s}p_{Z_{\mathrm{IM}}|\boldsymbol{\Theta}}\left(\ln x,t_{\mathrm{f}}\middle|\boldsymbol{\theta}\right)p_{Z_{\mathrm{EDP}}|\boldsymbol{\Theta}}\left(\ln z,t_{\mathrm{f}}\middle|\boldsymbol{\theta}\right)p_{\boldsymbol{\Theta}}(\boldsymbol{\theta})\,\mathrm{d}\boldsymbol{\theta}\\ &=\frac{1}{xz}\sum_{q=1}^{n}\int_{\Omega^{(q)}}p_{Z_{\mathrm{IM}}|\boldsymbol{\Theta}}\left(\ln x,t_{\mathrm{f}}\middle|\boldsymbol{\theta}\right)p_{Z_{\mathrm{EDP}}|\boldsymbol{\Theta}}\left(\ln z,t_{\mathrm{f}}\middle|\boldsymbol{\theta}\right)p_{\boldsymbol{\Theta}}(\boldsymbol{\theta})\,\mathrm{d}\boldsymbol{\theta}\\ &\doteq\frac{1}{xz}\sum_{q=1}^{n}p_{Z_{\mathrm{IM}}|\boldsymbol{\Theta}}\left(\ln x,t_{\mathrm{f}}\middle|\boldsymbol{\theta}^{(q)}\right)p_{Z_{\mathrm{EDP}}|\boldsymbol{\Theta}}\left(\ln z,t_{\mathrm{f}}\middle|\boldsymbol{\theta}^{(q)}\right)\int_{\Omega^{(q)}}p_{\boldsymbol{\Theta}}(\boldsymbol{\theta})\,\mathrm{d}\boldsymbol{\theta}\\ &=\frac{1}{xz}\sum_{q=1}^{n}\frac{1}{P_q}p_{Z_{\mathrm{IM}}}^{(q)}(\ln x,t_{\mathrm{f}})\,p_{Z_{\mathrm{EDP}}}^{(q)}(\ln z,t_{\mathrm{f}}).\end{aligned} \tag{24}$$

Meanwhile, the marginal PDF of IM can be given as

$$p_{\mathrm{IM}}(x)=\frac{1}{x}\int_{\mathbb{R}^s} p_{Z_{\mathrm{IM}}\boldsymbol{\Theta}}(\ln x,\boldsymbol{\theta},t_{\mathrm{f}})\,\mathrm{d}\boldsymbol{\theta}=\frac{1}{x}\sum_{q=1}^{n}\int_{\Omega^{(q)}} p_{Z_{\mathrm{IM}}|\boldsymbol{\Theta}}(\ln x,t_{\mathrm{f}}|\boldsymbol{\theta})\,p_{\boldsymbol{\Theta}}(\boldsymbol{\theta})\,\mathrm{d}\boldsymbol{\theta}$$
$$\doteq\frac{1}{x}\sum_{q=1}^{n} p_{Z_{\mathrm{IM}}\boldsymbol{\Theta}}\left(\ln x,t_{\mathrm{f}}|\boldsymbol{\theta}^{(q)}\right)\int_{\Omega^{(q)}} p_{\boldsymbol{\Theta}}(\boldsymbol{\theta})\,\mathrm{d}\boldsymbol{\theta}=\frac{1}{x}\sum_{q=1}^{n} p_{Z_{\mathrm{IM}}}^{(q)}(\ln x,t_{\mathrm{f}}). \tag{25}$$

Then, the fragility function in Eq. (20) can be calculated as

$$F(x;b)=\int_b^{\infty}\frac{p_{\mathrm{IM,EDP}}(x,z)}{p_{\mathrm{IM}}(x)}\mathrm{d}z\doteq\frac{1}{\sum_{q=1}^{n} p_{Z_{\mathrm{IM}}}^{(q)}(\ln x,t_{\mathrm{f}})}\int_b^{\infty}\frac{1}{z}\sum_{q=1}^{n}\frac{1}{P_q}\,p_{Z_{\mathrm{IM}}}^{(q)}(\ln x,t_{\mathrm{f}})\,p_{Z_{\mathrm{EDP}}}^{(q)}(\ln z,t_{\mathrm{f}})\mathrm{d}z. \tag{26}$$

The flowchart of the numerical implementation steps is shown in Fig. 1. The process outlined within the blue dashed box in the diagram represents the portion that requires parallel computations for each representative point of the basic random vector, while the process boxes highlighted in red bold indicate the key steps of employing the decoupled M-PDEM.

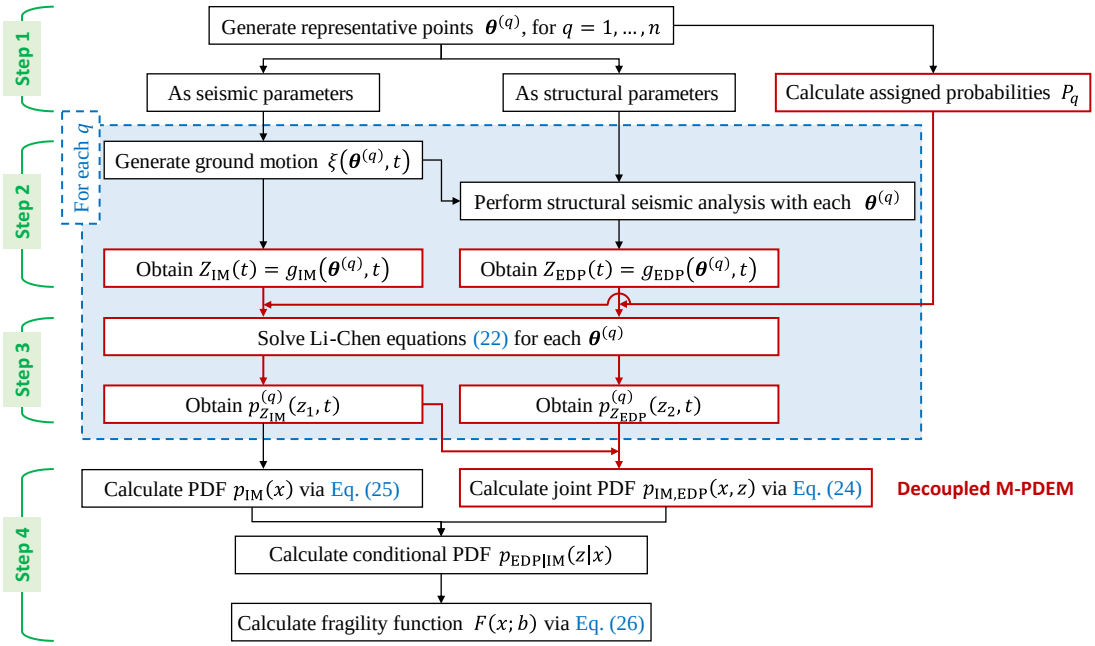

Fig. 1. Flowchart of cloud-based fragility analysis via decoupled M-PDEM.

5. Numerical verification

This section applies the proposed method to a practical engineering case study, conducting seismic fragility analysis on a three-span six-story RC frame structure under non-stationary stochastic seismic excitations. A comparison and validation of the results are performed against those obtained from MCS.

5.1. Non-stationary stochastic ground motion characterization

In the practical case, the non-stationary stochastic ground motion acceleration $\xi(\boldsymbol{\Theta},t)$ is modelled by the evolutionary power spectral density (PSD) given as (Deodatis 1996)

$$S_{\xi}(\omega,t)=\left(\frac{t}{t_{\mathrm{a}}}e^{1-\frac{t}{t_{\mathrm{a}}}}\right)^{\beta_{\mathrm{a}}}\frac{\bar{\xi}_{\mathrm{m}}^{2}\left[\omega_{\mathrm{g}}^{4}(t)+4\zeta_{\mathrm{g}}^{2}(t)\omega_{\mathrm{g}}^{2}(t)\omega^{2}\right]}{\pi\gamma^{2}\omega_{\mathrm{g}}(t)\left[2\zeta_{\mathrm{g}}(t)+\frac{1}{2\zeta_{\mathrm{g}}(t)}\right]\left\{\left[\omega^{2}-\omega_{\mathrm{g}}^{2}(t)\right]^{2}+4\zeta_{\mathrm{g}}^{2}(t)\omega_{\mathrm{g}}^{2}(t)\omega^{2}\right\}}\cdot\frac{\omega^{4}}{\left[\omega^{2}-0.01\omega_{\mathrm{g}}^{2}(t)\right]^{2}+0.04\zeta_{\mathrm{g}}^{2}(t)\omega_{\mathrm{g}}^{2}(t)\omega^{2}}, \tag{27}$$

where

$$\omega_{\mathrm{g}}(t)=\omega_{0}-\frac{\omega_{1}t}{t_{\mathrm{f}}},\text{and }\zeta_{\mathrm{g}}(t)=\zeta_{0}-\frac{\zeta_{1}t}{t_{\mathrm{f}}}; \tag{28}$$

the parameters are taken as $t_{\mathrm{f}}=25$ s, $t_{\mathrm{a}}=6$ s, $\beta_{\mathrm{a}}=2$, $\bar{\xi}_{\mathrm{m}}=1.96\ \mathrm{m/s^{2}}$, $\gamma=2.85$, $\omega_{0}=16\ \mathrm{s^{-1}}$, $\omega_{1}=5\ \mathrm{s^{-1}}$, $\zeta_{0}=0.6$, and $\zeta_{1}=0.2$.

According to the given evolutionary PSD model, the representative histories of the non-stationary stochastic ground motion can be generated by the SHF as (Chen et al. 2017, 2020a)

$$\xi(\boldsymbol{\Theta},t)=\sum_{k=1}^{n_{\mathrm{SHF}}}\sqrt{2S_{\xi}\left[\tilde{\omega}_{k}(\Lambda),t\right]\Delta\omega_{k}}\cos\left[\tilde{\omega}_{k}(\Lambda)t+\Phi_{k}\right], \tag{29}$$

where n_{SHF} is the number of numerical discretization intervals in the frequency domain $\omega\in[0,\omega_{\mathrm{f}}]=\left[\omega_{0},\omega_{n_{\mathrm{SHF}}}\right]$; $\Delta\omega_{k}=\omega_{k}-\omega_{k-1}$, in which the discretized interval $[\omega_{k-1},\omega_{k}]$ satisfies

$$\int_{\omega_{k-1}}^{\omega_{k}}\int_{0}^{t_{\mathrm{f}}}S_{\xi}(\omega,t)\mathrm{d}t\mathrm{d}\omega=\frac{1}{n_{\mathrm{SHF}}}\int_{\omega_{0}}^{\omega_{n_{\mathrm{SHF}}}}\int_{0}^{t_{\mathrm{f}}}S_{\xi}(\omega,t)\mathrm{d}t\mathrm{d}\omega,\text{for }k=1,\ldots,n_{\mathrm{SHF}}; \tag{30}$$

$\tilde{\omega}_{k}(\Lambda)$ takes

$$\tilde{\omega}_{k}(\Lambda)=\omega_{k-1}+\left[\omega_{k}-\omega_{k-1}\right]\Lambda,\text{for }k=1,\ldots,n_{\mathrm{SHF}}; \tag{31}$$

Φ_{k}, for $k=1,\ldots,n_{\mathrm{SHF}}$, and Λ are $(n_{\mathrm{SHF}}+1)$ uniform-distributed independent random variables in $[0,2\pi]$ and $[0,1]$, respectively, and they are the components of the basic random vector $\boldsymbol{\Theta}_{\mathrm{excit}}=\left(\Theta_{1},\cdots,\Theta_{n_{\mathrm{SHF}}},\Lambda\right)^{\mathrm{T}}$.

The numerical parameters are taken as $n_{\mathrm{SHF}}=10$ and $\omega_{\mathrm{f}}=2\pi/\Delta t$ in generation, and the time step is $\Delta t=0.05$ s. The evolutionary PSD model and the corresponding generated typical ground motion history are illustrated in Fig. 2.

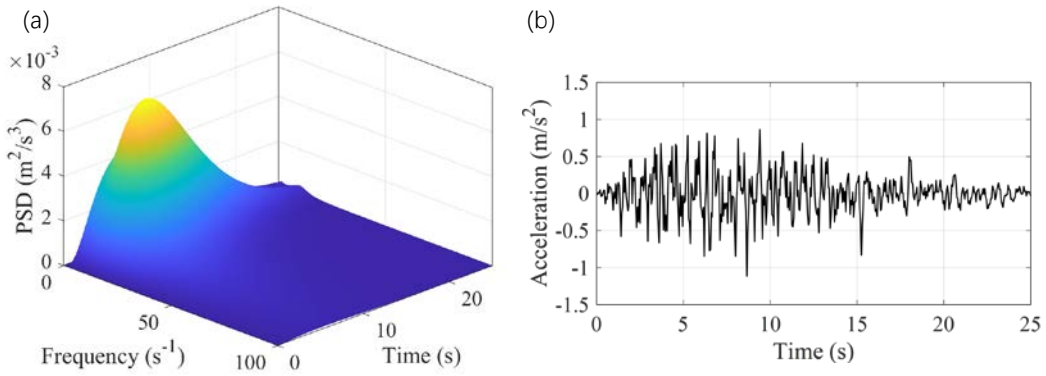

Fig. 2. Non-stationary stochastic ground motion:

(a) Evolutionary PSD; (b) Typical ground motion generation.

5.2. Three-span six-story RC frame structure modelling and analysis

In the present paper, a six-story three-span RC frame structure are employed for case study. The structure has a total of six stories with a design height of 22.5 m. Each span has a span length of 5.2 m, and there are a total of three spans. The geometric information and the cross-section and reinforcement details for each story of the structure are shown in Fig. 3.

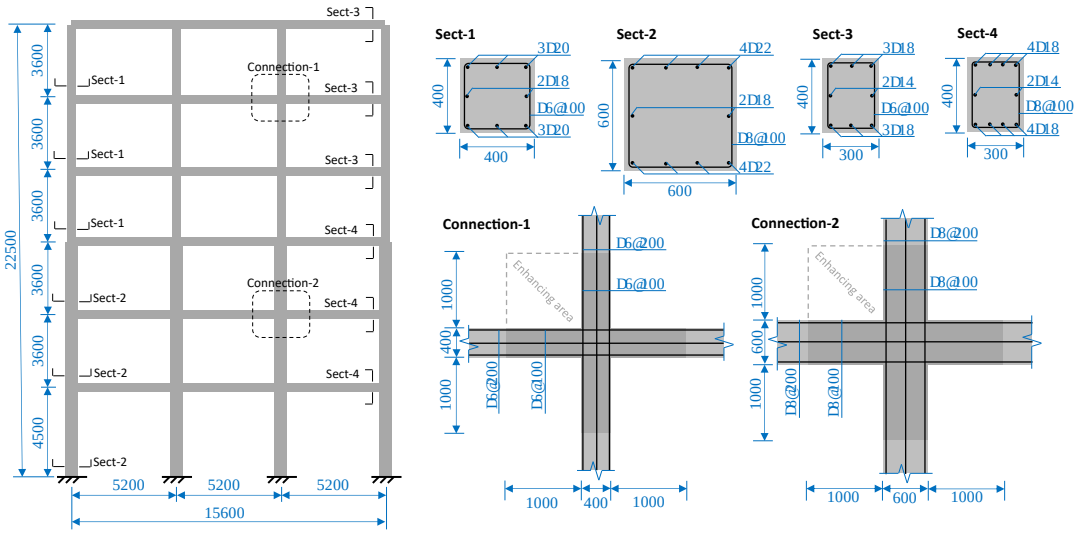

Fig. 3. Three-span six-story RC frame structure (unit: mm).

The structure employs reinforcing steel of grade HRB335, stirrups of grade HRB300, and concrete of grade C30. The damping ratio ζ_s, concrete compressive strength f_c, and peak compressive strain ε_c of the structure are considered as basic random parameters, namely, $\boldsymbol{\Theta}_{\text{param}} = \left(\zeta_s, f_c, \varepsilon_c\right)^{\mathrm{T}}$. Then, the seismic-structural system includes 14 independent basic random variables, i.e, $\boldsymbol{\Theta} = \left(\boldsymbol{\Theta}_{\text{param}}{}^{\mathrm{T}}, \boldsymbol{\Theta}_{\text{excit}}{}^{\mathrm{T}}\right)^{\mathrm{T}} = \left(\zeta_s, f_c, \varepsilon_c, \Phi_1, \cdots, \Phi_{n_{\text{SHF}}}, \Lambda\right)^{\mathrm{T}}$. These variables follow probability distributions with their respective distribution parameters (Lu et al. 2014, Chen et al. 2020a, Tao et al. 2020), as presented in Tab. 1.

Tab. 1. Basic random variables and their distributions.

Variables	Distribution	Parameters	PDF (Θ denoting each variable)
ζ_s	Gaussian	$\mu_{\zeta_s} = 0.05$, $\sigma_{\zeta_s} = 0.005$	$p_\Theta(\theta) = \frac{1}{\sqrt{2\pi}\sigma_\Theta} e^{-\frac{(\theta-\mu_\Theta)^2}{2\sigma_\Theta{}^2}}$
f_c (Pa)	Lognormal	$r_{f_c} = 3.4\times10^7$ Pa, $\sigma_{f_c} = 0.21$	$p_\Theta(\theta) = \frac{1}{\sqrt{2\pi}\sigma_\Theta\theta} e^{-\frac{1}{2\sigma_\Theta{}^2}\ln^2\frac{\theta}{r_\Theta}}$, for $\theta > 0$
ε_c	Lognormal	$r_{\varepsilon_c} = 2.2\times10^{-3}$, $\sigma_{\varepsilon_c} = 0.17$	
Φ_k, for $k = 1, \ldots, n_{\text{SHF}}$	Uniform	$[a_\Phi, b_\Phi] = [0, 2\pi]$	$p_\Theta(\theta) = \frac{1}{b_\Theta - a_\Theta}$, for $a_\Theta < \theta < b_\Theta$
Λ	Uniform	$[a_\Theta, b_\Theta] = [0, 1]$	

The modeling methodology adopted for the practical application example involves the utilization of nonlinear

beam-column elements and specialized node elements. These elements serve as fundamental building blocks in the analysis and are integral to capturing the intricate nonlinear behavior of the structural system.

The nonlinear beam-column elements, generated using the flexibility method, play a central role in characterizing the force-based nonlinearity exhibited by structural members. These elements remain stable under conditions of pronounced nonlinearity, enabling them to accurately represent the complex response of the structure. Each integration point within these elements is furnished with fiber sections representing both steel and concrete fibers (Scott et al. 1982). This delineation enables the precise modeling of mechanical properties within the structure.

Moreover, the analysis employs specialized node elements to accurately model the behavior of critical regions such as beam-column joints. The joint two-dimensional element, a key component, incorporates a central spring and four interfacial springs (Bentz et al. 2006). The central spring characterizes shear damage in the core zones. This material model's parameters are derived from the modified compression field theory, which captures the interfacial moment-rotation relationship. The interfacial springs, on the other hand, simulate the bond-slip effects of reinforcement and are described using the hysteresis material model (Cao et al. 2022). The parameters of this model are obtained through zero-length fiber-section analysis, capturing the joint moment-rotation relationship.

After generating representative points for the basic random vector $\boldsymbol{\Theta}$, these points are employed as inputs for the structural parameters. Furthermore, the generated representative seismic excitations are applied as inputs to the structure. Dynamic analyses of the finite element method (FEM) model are then conducted using the OpenSEES software, facilitating the acquisition of response time histories for the structure under each representative points.

5.3. Seismic fragility analysis

In this case study, 800 representative points for the basic random vector $\boldsymbol{\Theta}$ are utilized to generate non-stationary random seismic excitations., i.e., $n = 800$ These excitations are subsequently employed as input for dynamic FEM analyses of the structure. Obtained numerical solutions of the response quantities of interest under each representative point are then substituted into the Li-Chen equation (22) for numerical solution. The decoupled M-PDEM is employed to provide the joint PDF of IM and EDP for the seismic-structural system, as well as the conditional PDF of EDP under the given IM.

The results of the joint PDF of IM and EDP and the conditional PDF of EDP given IM are illustrated in Figs. 4 and 5, respectively, via PDF surfaces and contours, where black scattered points in Fig. 4 (b) represent numerical solutions of IM and EDP under representative points. The different curves in Fig. 5 (c) represent the conditional PDFs of EDP under various given IM, including IM = 0.5 g, 1.0 g, 2.0 g, and 4.0 g. These PDFs do not need to be separately computed for different IM values; instead, they can be obtained comprehensively through the decoupled M-PDEM analysis in a single step. Traditional cloud analyses typically model this conditional distribution using the lognormal distribution. However, as evident from Fig. 5 (c), the results obtained from the decoupled M-PDEM analysis exhibit significant deviations from the lognormal distribution. The accuracy of the decoupled M-PDEM analysis will be validated next, and its detailed comparison and discussion with the traditional cloud method will be presented in Sec. 6.

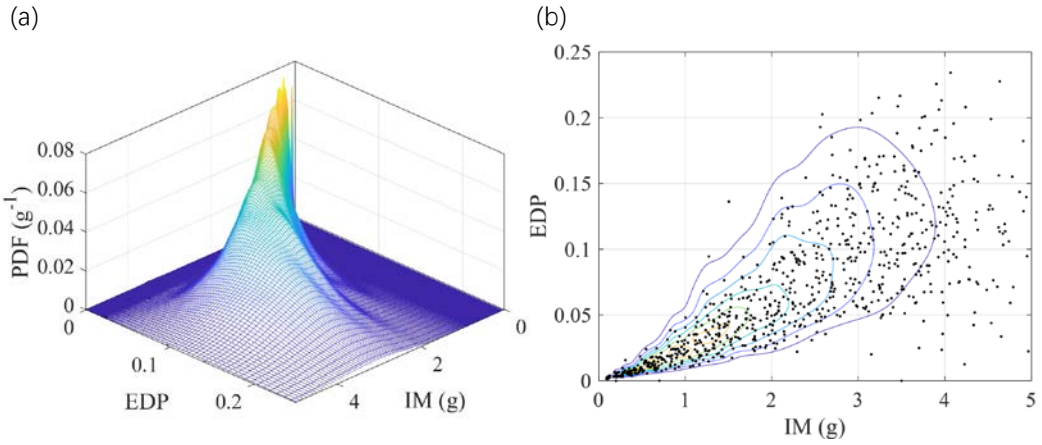

Fig. 4. Joint PDF of IM and EDP:
(a) Joint PDF surface; (b) Joint PDF contour.

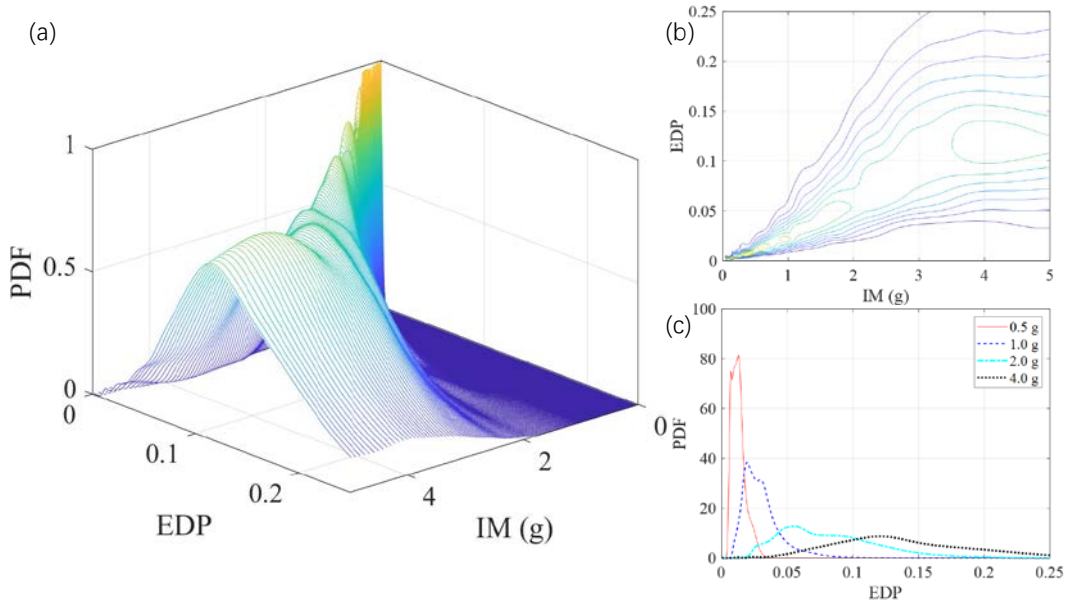

Fig. 5. Conditional PDF of EDP given IM:
(a) Conditional PDF surface; (b) Conditional PDF contour; (c) Conditional PDFs under various given IMs.

Integrating the conditional PDF with respect to EDP within the failure domain yields the fragility varying with IM. The fragility curves for different limit state models are illustrated in Fig. 6. Four limit state models, i.e., slight, moderate, extensive, and complete, are considered through various failure thresholds of EDP (Jeon et al. 2015). The curves of varying colors and line styles represent the fragility obtained from decoupled M-PDEM analysis at different thresholds. The corresponding scatter points depict the fragility obtained from MCS at different thresholds. The MCS results involve performing 10^4 stochastic dynamic analysis simulations for the seismic-structural system at each IM value, and a total of 2×10^5 stochastic samples are needed to obtain the entire fragility curve. This serves as a comparison to the proposed method. Figs. 6 (a) and (b) present the comparison results of failure probability in linear and logarithmic coordinates, respectively. It is evident that the decoupled M-PDEM analysis results based on 800 representative analyses match closely with the MCS results of 2×10^5 samples, even in the region of low failure probabilities displayed on the logarithmic scale. This validates the high computational accuracy of cloud-based

fragility analysis via the decoupled M-PDEM. It is also noticed a slight fluctuation in the red solid curve around the order of 10^{-2} in Fig. 6 (b), indicating a non-monotonic behavior in the presented fragility curve. This fluctuation is attributed to numerical errors. Diverging from traditional empirical fragility models, the proposed method is non-parametric and does not inherently assume the monotonicity of the fragility curve. However, from the numerical results, it is evident that, except for a slight numerical fluctuation, the proposed method nearly perfectly adheres to monotonicity in the computed fragility curve. This further validates that the numerical results provided by the proposed method, driven by physical mechanisms, are highly accurate in qualitative analysis.

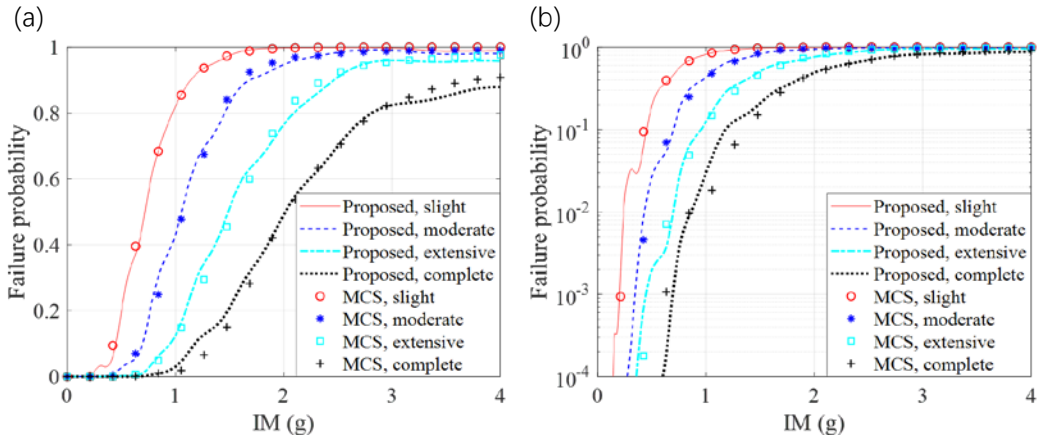

Fig. 6. Fragility via decoupled M-PDEM:
(a) Linear coordinate; (b) Logarithmic coordinate.

6. Results and discussion

To further compare the convergence of the fragility analysis results obtained using the proposed method with increasing representative analysis quantities, representative point numbers n were selected as 120, 200, 400, and 800. Seismic excitations were generated, structural dynamic analyses were conducted, and Li-Chen equations were solved for different representative point quantities. The resulting fragility curves were then compared with the MCS, as depicted in Fig. 7 shown by the solid curves and hollow dots, respectively. It can be observed that as the number of representative analyses increases, the fragility curves obtained through decoupled M-PDEM analysis become increasingly close to the MCS results.

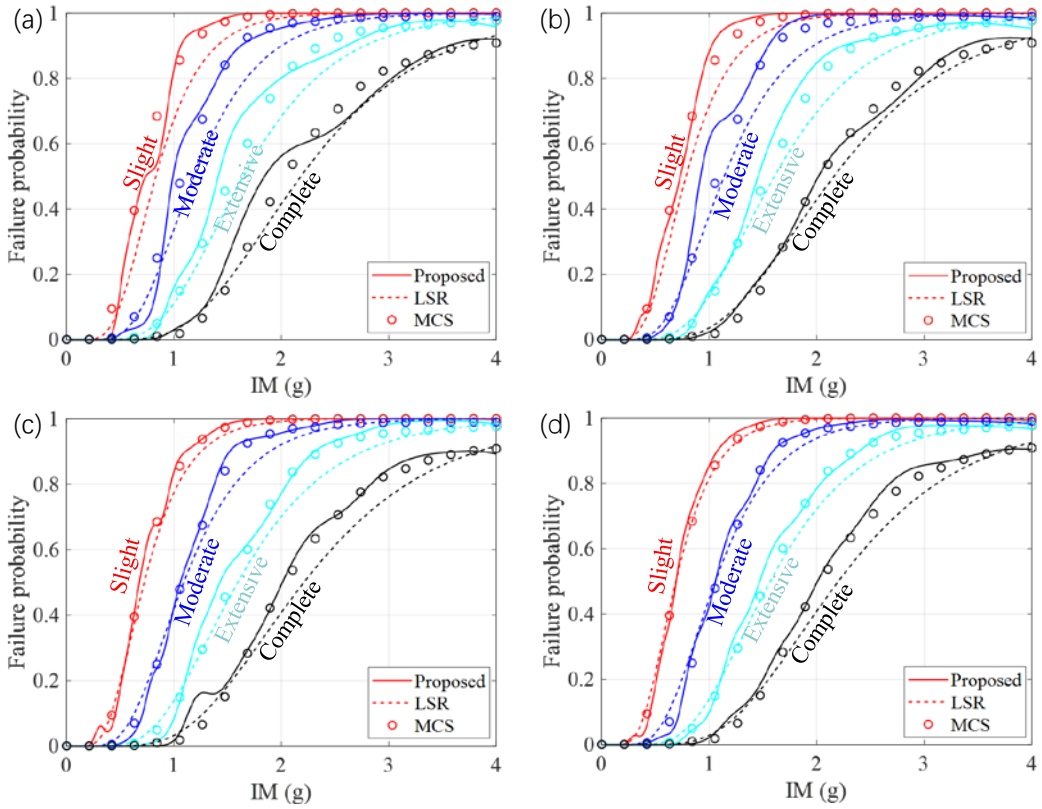

Fig. 7. Fragility comparison based on various number of representative analyses: (a) $n=120$; (b) $n=200$; (c) $n=400$; (d) $n=800$.

In order to quantify the accuracy of the fragility curves, the error estimation formula can be introduced as (Feng et al. 2023)

$$\text{error}=\frac{1}{k}\sum_{j=1}^{k}\sqrt{\frac{1}{IM_{\text{u}}}\int_{0}^{IM_{\text{u}}}\left[\tilde{F}\left(x;b_j\right)-F\left(x;b_j\right)\right]^2\text{d}x}, \tag{32}$$

where $F\left(\cdot\right)$ represents the exact solution of the fragility function, which is given by 2×10^5 MCS results; $\tilde{F}\left(\cdot\right)$ represents the fragility function calculated by the proposed method; IM_{u} is the upper bound of the IM, set to 4 g; b_j, for $j=1,\ldots,k$, represent different failure threshold corresponding to the four limit state models. The second row in Tab. 2 presents the errors of the fragility functions obtained through decoupled M-PDEM analysis for different numbers of representative analyses. It can be observed that as the number of representative analyses increases, the errors gradually decrease.

Tab. 2. Error comparison of various fragility results.

n	120	200	400	800
Decoupled M-PDEM	0.0417	0.0291	0.0210	0.0183
LSR	0.0528	0.0448	0.0352	0.0375

To further demonstrate the advance of the proposed method in terms of computational accuracy and efficiency, a comparison is made between the results obtained using the proposed method and those obtained through traditional cloud analysis, i.e., estimating conditional mean parameters through LSR and fitting EDP's conditional distribution under IM with a lognormal distribution, under 120, 200, 400, and 800 representative analyses respectively, as shown

in Fig. 7 by dashed curves as well. The fragility obtained from 800 representative analyses combined with decoupled M-PDEM analysis exhibit significantly higher accuracy compared to them obtained from the same number of representative analyses combined with the LSR.

Fig. 8 depict the log conditional means of EDP under IM obtained from the decoupled M-PDEM analysis and the LSR, where the black dots represent data points obtained from 800 deterministic analyses of IM and EDP; The red solid line represents the conditional mean of lnEDP under IM, and the magenta dashed line represents the conditional mean plus and minus one STD. The log conditional mean and STD via the LSR are estimated by Eqs. (1) and (4), respectively, while them via the decoupled M-PDEM are determined by the conditional PDF, namely,

$$\mu_{\ln \mathrm{D}}(x) = \mathrm{E}\left(\ln EDP \,\middle|\, IM = x\right) = \int_0^\infty z p_{Z_{\mathrm{MIDA}}|Z_{\mathrm{PGA}}}\left(z \,|\ln x, t_{\mathrm{f}}\right)\mathrm{d}z, \tag{33}$$

and

$$\sigma_{\ln \mathrm{D}}(x) = \sqrt{\mathrm{Var}\left(\ln EDP \,\middle|\, IM = x\right)} = \sqrt{\int_0^\infty \left[z - \mu_{\ln \mathrm{D}}(x)\right]^2 p_{Z_{\mathrm{MIDA}}|Z_{\mathrm{PGA}}}\left(z \,|\ln x, t_{\mathrm{f}}\right)\mathrm{d}z}. \tag{34}$$

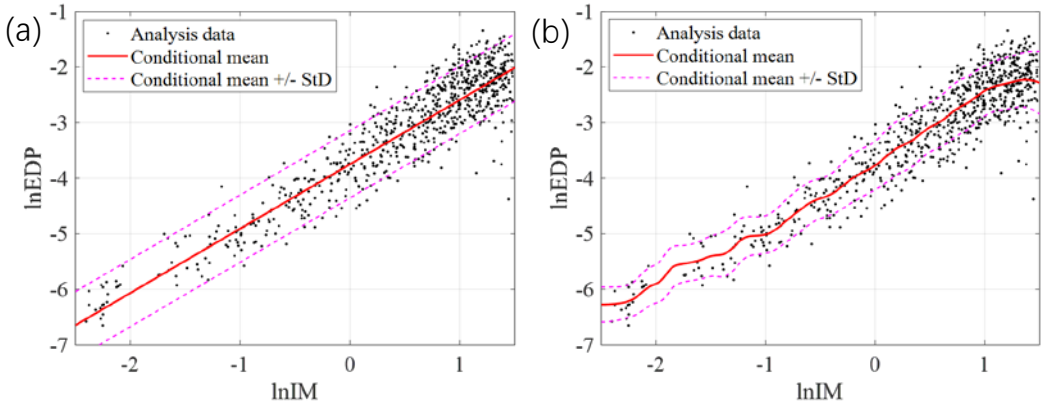

Fig. 8. Log conditional mean of EDP given IM:
(a) Decoupled M-PDEM; (b) LSR.

In fact, when conducting fragility analysis using the decoupled M-PDEM, there is no need to compute conditional mean and STD. Instead, the joint PDF and conditional PDF are directly obtained by solving the Li-Chen equations. Here, the conditional mean and STD are derived from the obtained conditional PDF to compare with from the LSR. Comparing Figs. 8 (a) and (b), it can be observed that the conditional means by the decoupled M-PDEM exhibit a nearly identical linear relationship with the LSR results, with minor differences. However, the significant difference in the fragility between the two methods can be seen in Fig. 7 (d).

This difference arises because conditional means and STDs represent an analysis level from statistical moments, while fragility, as obtained by the integral of the conditional PDF within the failure domain, reflects an analysis level from probability density. When the accuracy of fitting statistical moments is acceptable, the corresponding probability density estimates may not be as accurate. This is because the process of transforming statistical moments into probability density introduces additional assumptions as outlined in Assumption 2 in Subsec. 2.1, which can lead to larger errors in the fragility results obtained from LSR. On the other hand, the decoupled M-PDEM analysis directly solves the Li-Chen equations with physics-driven perspective. It provides more accurate results at the probability density level and thus demonstrating a considerable advantage in terms of accuracy.

The third row in Tab. 2 also presents the errors of fragility obtained by the LSR for different representative analysis quantities. The error comparison is also shown in Fig. 9. It can be observed that the convergence of errors in

fragility analysis by LSR is not evident as the number of representative analyses increases. In some cases, such as with 800 points, the error is even higher than that with 400 points. This discrepancy arises because, regardless of the number of representative analyses conducted, the traditional cloud analysis based on the LSR, as outlined in Subsec. 2.1 with its three assumptions, provides empirically approximate fragility results. Consequently, it cannot achieve higher levels of analysis accuracy. In contrast, the fragility obtained by the decoupled M-PDEM exhibit noticeably smaller computational errors, and with an increasing number of representative analyses, the errors gradually diminish.

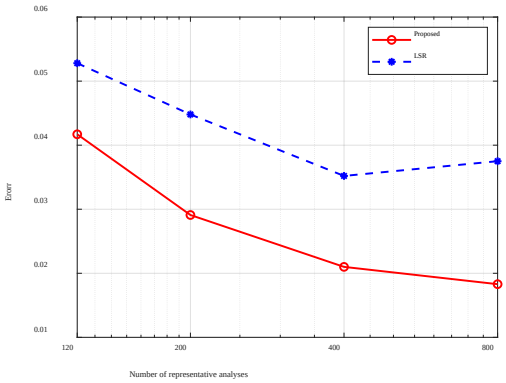

Fig. 9. Error comparison of various fragility results.

Remark 2 (Limitation and future works): While our proposed method exhibits notable advantages in terms of numerical precision and efficiency, it is crucial to acknowledge certain limitations inherent in its application. One significant consideration is the requirement to solve PDEs, albeit in a one-dimensional context. This necessitates a deeper theoretical understanding compared to traditional fragility methods. However, it is essential to underscore that the derived fragility function [Eq. (20)] is rigorously formulated without relying on empirical assumptions, ensuring heightened result accuracy. Additionally, the method's application in seismic fragility assessment has been explored in a preliminary manner, and its versatility requires further investigation. Specifically, its suitability in scenarios involving multiple damage states or vector-valued IMs (Zhou et al. 2017, Du & Padgett 2020, Jalayer et al. 2023) warrants additional scrutiny. These limitations serve as avenues for future research, aiming to enhance the method's applicability and address diverse structural scenarios.

7. Concluding remarks

In this study, a novel approach to seismic fragility analysis within a performance-based earthquake engineering (PBEE) framework has been proposed. This method, based on the cloud analysis, distinguishes itself from traditional methods by utilizing the decoupled joint probability density evolution method (M-PDEM) to calculate the joint probability density functions (PDFs) of intensity measure (IM) and engineering demand parameter (EDP). IM and EDP are fundamental response quantities of the seismic-structural system, and their transient PDFs satisfy a class of one-dimensional partial differential equations (PDEs) known as Li-Chen equations. By employing the decoupled M-PDEM to solve these equations, the joint PDFs of IM and EDP, as well as the conditional PDFs of EDP given IM, can be obtained, leading to seismic fragility results. The method exhibits high numerical precision and computational efficiency. Key conclusions of this study include:

(1) The decoupled M-PDEM provides a methodology to solve the one-dimensional Li-Chen equations governing the temporal evolution of the transient PDFs of both the time-variant peak ground acceleration (PGA) process and structural extreme value response process subject to stochastic seismic excitations. The joint PDF of IM

and EDP can be obtained by solving their respective one-dimensional Li-Chen equations, avoiding the computational burden associated with high-dimensional PDE solving.

(2) The use of decoupled M-PDEM for cloud-based seismic fragility analysis demonstrates superior computational accuracy. It achieves close agreement with the results of 10^5 Monte Carlo simulations (MCSs) using representative analysis data on the order of 10^2. Additionally, it offers high accuracy in capturing the tail of fragility under logarithmic coordinates, particularly for small probability of failure events. This precision arises from the fact that the joint PDF required for fragility analysis is physically driven by the Li-Chen equations and incorporates contributions from representative analysis data, surpassing the accuracy of solely data-driven fitting.

(3) Compared to traditional cloud analysis based on least squares regression (LSR), the decoupled M-PDEM exhibits higher computational accuracy at similar structural analysis costs. This is due to the method's direct acquisition of conditional PDF information through the solution of physics-driven Li-Chen equations, offering greater precision assurance than data-driven fitting combined with empirical assumptions.

In summary, this study presents a methodology, numerical strategy, and validation under benchmark models for seismic fragility analysis via the decoupled M-PDEM. The proposed method can be further extended to address fragility assessment involving multiple damage states and vector-valued IMs. Additionally, the proposed method allows for the analysis of confidence intervals for fragility curves. This approach can be extended to more complex engineering structures, including the fragility and resilience analyses of high-rise buildings, long-span bridges, and of under sequence-type seismic excitations.

Acknowledgements

Financial supports from the Project of National Key Research and Development Program of China (Grant No. 2022YFC3803004), the National Natural Science Foundation of China (Grant No. 12302037), China Postdoctoral Science Foundation (Grant No. 2023M732669), Shanghai Post-Doctoral Excellence Program (Grant No. 2022558), and the Natural Science Foundation of Jiangsu Province (Grant No. BK20220984) are highly appreciated. Prof. Jian-Bing Chen from Tongji University is gratefully appreciated for his constructive comments and encouragement.

Data availability

The datasets generated during and/or analyzed during the current study are available from the corresponding author on reasonable request.

Declaration

The authors have no conflicts of interest to declare that are relevant to the content of this article.

Author Statement

Meng-Ze Lyu: Methodology; Software; Formal analysis; Investigation; Writing - Original draft; Funding acquisition. **De-Cheng Feng**: Conceptualization; Resources; Visualization; Writing - Review & editing; Funding acquisition. **Xu-Yang Cao**: Data Curation; Visualization; Writing - Review & editing. **Michael Beer**: Writing - Review & editing; Supervision.

References

[1] Afshari SS, Pourtakdoust SH, 2018. Probability density evolution for time-varying reliability assessment of wing structures [J]. Aviation, 22 (2): 45-54.

[2] Altieri D, Patelli E, 2020. An efficient approach for computing analytical non-parametric fragility curves [J]. Structural Safety, 85: 101956.

[3] Ang AHS, De Leon D, Fan WL, 2021. Optimal reliability-based design of complex structural systems [J]. Structural Safety, 90: 102048.
[4] Baker JW, 2015. Efficient analytical fragility function fitting using dynamic structural analysis [J]. Earthquake Spectra, 31 (1): 579-599.
[5] Bentz EC, Vecchio FJ, Collins MP, 2006. Simplified modified compression field theory for calculating shear strength of reinforced concrete elements [J]. ACI Structural Journal, 103 (4): 614.
[6] Cao XY, Xiong CZ, Feng DC, Wu G, 2022. Dynamic and probabilistic seismic performance assessment of precast prestressed reinforced concrete frames incorporating slab influence through three-dimensional spatial model [J]. Bulletin of Earthquake Engineering, 2022: 1-35.
[7] Cao XY, Feng DC, Beer M, 2023a. Consistent seismic hazard and fragility analysis considering combined capacity-demand uncertainties via probability density evolution method [J]. Structural Safety, 103: 102330.
[8] Cao XY, Feng DC, Beer M, 2023b. A KDE-based non-parametric cloud approach for efficient seismic fragility estimation of structures under non-stationary excitation [J]. Mechanical Systems & Signal Processing (under review).
[9] Cao XY, Feng DC, Li Y, 2023c. Assessment of various seismic fragility analysis approaches for structures excited by non-stationary stochastic ground motions [J]. Mechanical Systems & Signal Processing, 186: 109838.
[10] Chen GH, Yang DX, 2019. Direct probability integral method for stochastic response analysis of static and dynamic structural systems [J]. Computer Methods in Applied Mechanics & Engineering, 357: 112612.
[11] Chen JB, Ghanem R, Li J, 2009. Partition of the probability-assigned space in probability density evolution analysis of nonlinear stochastic structures [J]. Probabilistic Engineering Mechanics, 24 (1): 27-42.
[12] Chen JB, Li J, 2009. A note on the principle of preservation of probability and probability density evolution equation [J]. Probabilistic Engineering Mechanics, 24 (1): 51-59.
[13] Chen JB, Sun WL, Li J, Xu J, 2013. Stochastic harmonic function representation of stochastic processes [J]. Journal of Applied Mechanics, 80: 011001.
[14] Chen JB, Yang JY, Li J, 2016. A GF-discrepancy for point selection in stochastic seismic response analysis of structures with uncertain parameters [J]. Structural Safety, 59: 20-31.
[15] Chen JB, Kong F, Peng YB, 2017. A stochastic harmonic function representation for non-stationary stochastic processes [J]. Mechanical Systems & Signal Processing, 96: 31-44.
[16] Chen JB, Comerford L, Peng YB, Beer M, Li J, 2020a. Reduction of random variables in the stochastic harmonic function representation via spectrum-relative dependent random frequencies [J]. Mechanical Systems & Signal Processing, 141: 106718.
[17] Chen JB, Yang JS, Jensen H, 2020b. Structural optimization considering dynamic reliability constraints via probability density evolution method and change of probability measure [J]. Structural & Multidisciplinary Optimization, 62 (5): 2499-2516.
[18] Choi E, DesRoches R, Nielson B, 2004. Seismic fragility of typical bridges in moderate seismic zones [J]. Engineering Structures, 26 (2): 187-199.
[19] Cornell CA, Jalayer F, Hamburger RO, Foutch DA, 2002. Probabilistic basis for 2000 SAC federal emergency management agency steel moment frame guidelines [J]. Journal of Structural Engineering, 128 (4): 526-533.
[20] Das S, Tesfamariam S, 2024. Reliability assessment of stochastic dynamical systems using physics informed neural network based PDEM [J]. Reliability Engineering & System Safety, 243: 109849.
[21] Deodatis G, 1996. Non-stationary stochastic vector processes: Seismic ground motion applications [J]. Probabilistic Engineering Mechanics, 11 (3): 149-167.
[22] Du A, Padgett JE, 2020. Investigation of multivariate seismic surrogate demand modeling for multi-response structural systems [J]. Engineering Structures, 207: 110210.
[23] Ellingwood BR, Rosowsky DV, Li Y, Kim JH, 2004. Fragility assessment of light-frame wood construction subjected to wind and earthquake hazards [J]. Journal of Structural Engineering, 130 (12): 1921-1930.
[24] Fan WL, Chen JB, Li J, 2009. Solution of generalized density evolution equation via a family of δ, sequences [J]. Chinese Journal of Theoretical & Applied Mechanics, 43 (6): 781.
[25] Feng DC, Cao XY, Wang D, Wu G, 2023. A PDEM-based non-parametric seismic fragility assessment method for RC structures under non-stationary ground motions [J]. Journal of Building Engineering, 63: 105465.
[26] Gardoni P, Der Kiureghian A, Mosalam KM, 2002. Probabilistic capacity models and fragility estimates for reinforced concrete columns based on experimental observations [J]. Journal of Engineering Mechanics, 128 (10): 1024-1038.
[27] Gasser C, Goldgruber M, Bucher C, 2019. Seismic fragility curves of an arch dam with special regard to ultimate limit state [J]. ASCE-ASME Journal of Risk & Uncertainty in Engineering Systems, Part B – Mechanical Engineering, 5 (4): 041002.
[28] Hai L, Lyu MZ, 2023. Modeling tensile failure of concrete considering multivariate correlated random fields of material parameters [J]. Probabilistic Engineering Mechanics (under review).
[29] Jalayer F, Cornell CA, 2009. Alternative nonlinear demand estimation methods for probability-based seismic assessments [J]. Earthquake Engineering & Structural Dynamics, 38 (8): 951-972.
[30] Jalayer F, De Risi R, Manfredi G, 2015. Bayesian cloud analysis: Efficient structural fragility assessment using linear regression [J]. Bulletin of Earthquake Engineering, 13: 1183-1203.

[31] Jalayer F, Ebrahimian H, Trevlopoulos K, Bradley B, 2023. Empirical tsunami fragility modelling for hierarchical damage levels [J]. Natural Hazards & Earth System Sciences, 23 (2): 909-931.
[32] Jeon JS, Shafieezadeh A, Lee DH, Choi E, DesRoches R, 2015. Damage assessment of older highway bridges subjected to three-dimensional ground motions: Characterization of shear–axial force interaction on seismic fragilities [J]. Engineering Structures, 87: 47-57.
[33] Jia GF, Taflanidis AA, 2014. Sample-based evaluation of global probabilistic sensitivity measures [J]. Computers & Structures, 144: 103-118.
[34] Kiani J, Camp C, Pezeshk S, 2019. On the application of machine learning techniques to derive seismic fragility curves [J]. Computers & Structures, 218: 108-122.
[35] Lallemant D, Kiremidjian A, Burton H, 2015. Statistical procedures for developing earthquake damage fragility curves [J]. Earthquake Engineering & Structural Dynamics, 44 (9): 1373-1389.
[36] Li J, Chen JB, 2004. Probability density evolution method for dynamic response analysis of structures with uncertain parameters [J]. Computational Mechanics, 34 (5): 400-409.
[37] Li J, Chen JB, 2008. The principle of preservation of probability and the generalized density evolution equation [J]. Structural Safety, 30 (1): 65-77.
[38] Li J, Chen JB, 2009. Stochastic Dynamics of Structure [M]. John Wiley & Sons, Singapore.
[39] Li J, Chen JB, Sun WL, Peng YB, 2012. Advances of the probability density evolution method for nonlinear stochastic systems [J]. Probabilistic Engineering Mechanics, 28 (4): 132-142.
[40] Li J, Wang D, 2022. Comparison of PDEM and MCS: Accuracy and efficiency [J]. Probabilistic Engineering Mechanics, 71, 103382.
[41] Liu DY, Lyu MZ, 2023. Uncertainty quantification for granular materials with a stochastic discrete element method [J]. Computers & Geotechnics, 161: 105560.
[42] Lu DG, Yu XH, Jia MM, Wang GY, 2014. Seismic risk assessment for a reinforced concrete frame designed according to Chinese codes [J]. Structure & Infrastructure Engineering, 10 (10): 1295-1310.
[43] Luo Y, Ai XQ, 2023. Wind risk assessment of urban street trees based on wind-induced fragility [J]. Disaster Prevention & Resilience, 1 (2): 7.
[44] Lyu MZ, Chen JB, 2022. A unified formalism of the GE-GDEE for generic continuous responses and first-passage reliability analysis of multi-dimensional nonlinear systems subjected to non-white-noise excitations [J]. Structural Safety, 98: 102233.
[45] Lyu MZ, Ai XQ, Sun TT, Chen JB, 2023a. Fragility analysis of curtain walls based on wind-borne debris considering wind environment [J]. Probabilistic Engineering Mechanics, 71: 103397.
[46] Lyu MZ, Chen JB, Shen JX, 2023b. Refined probabilistic response and seismic reliability evaluation of high-rise reinforced concrete structures via physically-driven GE-GDEE [J]. Acta Mechanica (online).
[47] Lyu MZ, Feng DC, Chen JB, Li J, 2024. A decoupled approach for determination of the joint probability density function of a high-dimensional nonlinear stochastic dynamical system via the probability density evolution method [J]. Computer Methods in Applied Mechanics & Engineering, 418: 116443.
[48] Mai CV, Konakli K, Sudret B, 2017. Seismic fragility curves for structures using non-parametric representations [J]. Frontiers of Structural & Civil Engineering, 11 (2): 169-186.
[49] Mangalathu S, Heo G, Jeon JS, 2018. Artificial neural network based multi-dimensional fragility development of skewed concrete bridge classes [J]. Engineering Structures, 162: 166-176.
[50] Moehle J, Deierlein GG, 2004. A framework methodology for performance-based earthquake engineering [C]. Proceedings of the 13th World Conference on Earthquake Engineering, Vancouver, Canada.
[51] Nielsen SRK, Peng YB, Sichani MT, 2016. Response and reliability analysis of nonlinear uncertain dynamical structures by the probability density evolution method [J]. International Journal of Dynamics & Control, 4 (2): 221-232.
[52] Nielson BG, DesRoches R, 2007. Seismic fragility methodology for highway bridges using a component level approach [J]. Earthquake Engineering & Structural Dynamics, 36 (6): 823-839.
[53] Padgett JE, Nielson BG, DesRoches R, 2008. Selection of optimal intensity measures in probabilistic seismic demand models of highway bridge portfolios [J]. Earthquake Engineering & Structural Dynamics, 37 (5): 711-725.
[54] Pang YT, Wang XW, 2021. Cloud-IDA-MSA conversion of fragility curves for efficient and high-fidelity resilience assessment [J]. Journal of Structural Engineering, 147 (5): 04021049.
[55] Papadopoulos V, Kalogeris I, 2016. A Galerkin-based formulation of the probability density evolution method for general stochastic finite element systems [J]. Computational Mechanics, 57 (5): 701-716.
[56] Porter KA, 2003. An overview of PEER's performance-based earthquake engineering methodology [C]. Proceedings of the 9th International Conference on Applications of Statistics & Probability in Civil Engineering, San Francisco, USA.
[57] Pourtakdoust SH, Khodabakhsh AH, 2022. A deep learning approach for the solution of probability density evolution of stochastic systems [J]. Structural Safety, 99: 102256.
[58] Priestley MJN, 2000. Performance based seismic design [J]. Proceedings of the 12th World Conference on Earthquake Engineering, Auckland, New Zealand.

[59] Scott BD, Park R, Priestley M, 1982. Stress-strain behavior of concrete confined by overlapping hoops at low and high strain rates [J]. Journal Proceedings, 79 (1): 13-27.
[60] Shafieezadeh A, Ramanathan K, Padgett JE, DesRoches R, 2012. Fractional order intensity measures for probabilistic seismic demand modeling applied to highway bridges [J]. Earthquake Engineering & Structural Dynamics, 41 (3): 391-409.
[61] Shinozuka M, Feng MQ, Lee JH, Naganuma T, 2000. Statistical Analysis of Fragility Curves [J]. Journal of Engineering Mechanics, 126 (12): 1224-1231.
[62] Singhal A, Kiremidjian AS, 1996. Method for probabilistic evaluation of seismic structural damage [J]. Journal of Structural Engineering, 122 (12): 1459-1467.
[63] Tao JJ, Chen JB, Ren XD, 2020. Copula-based quantification of probabilistic dependence configurations of material parameters in damage constitutive modeling of concrete [J]. Journal of Structural Engineering, 146 (9): 04020194.
[64] Vamvatsikos D, Cornell CA, 2002. Incremental dynamic analysis [J]. Earthquake Engineering & Structural Dynamics, 31 (3): 491-514.
[65] Wang D, Li J, 2020. A reproducing kernel particle method for solving generalized probability density evolution equation in stochastic dynamic analysis [J]. Computational Mechanics, 65 (3): 597-607.
[66] Wang D, Sun WL, Li J, 2021. An RKPM-based formulation of the generalized probability density evolution equation for stochastic dynamic systems [J]. Probabilistic Engineering Mechanics, 66: 103152.
[67] Wang M, Du XL, Sun FF, Nagarajaiah S, Li YW, 2022. Fragility analysis and inelastic seismic performance of steel braced-core-tube frame outrigger tall buildings with passive adaptive negative stiffness damped outrigger [J]. Journal of Building Engineering, 52: 104428.
[68] Wang ZY, Pedroni N, Zentner I, Zio E, 2018. Seismic fragility analysis with artificial neural networks: Application to nuclear power plant equipment [J]. Engineering Structures, 162: 213-225.
[69] Zhou Y, Ge PL, Han JP, Lu Z, 2017. Vector-valued intensity measures for incremental dynamic analysis [J]. Soil Dynamics & Earthquake Engineering, 100: 380-388.